Field Quality Measurement of a 4.2-m Long Prototype Low-β Nb_3Sn Quadrupole Magnet during the Assembly Stage for the High-Luminosity LHC Accelerator Upgrade Project

Xiaorong Wang, Giorgio F. Ambrosio, Daniel W. Cheng, Guram Chlachidze, Joseph DiMarco, William Ghiorso, Christopher Hernikl, Thomas M. Lipton, Scott Myers, Heng Pan, Soren O. Prestemon, GianLuca Sabbi

***Abstract*—The U.S. High-Luminosity LHC Accelerator Upgrade Project, in collaboration with CERN, is developing Nb_3Sn quadrupole magnets (MQXFA) to be installed at the interaction region of the LHC. The project will deliver 20 MQXFA magnets in 10 cold masses. These magnets need to meet the stringent requirements on field quality at the nominal operating current. Compared to the mature NbTi accelerator magnet technology, achieving excellent field quality can be challenging for Nb_3Sn magnets. To help track, understand, and allow effective correction of geometric field errors, field quality measurements at room temperature during the MQXFA assembly stage was planned for the project. The measurements also intend to evaluate the magnetic axis and twist angle along the magnet aperture. We report the first measurement on a prototype MQXFA magnet using a recently developed measurement system. The magnetic axis and twist angle met the acceptance criteria. Further development needs for the room-temperature measurements were discussed. We expect that statistics obtained from such measurements throughout the project will provide insight into future applications of high-performance Nb_3Sn accelerator magnets.**

***Index Terms*—Nb_3Sn accelerator magnets, field quality, High-Luminosity LHC Upgrade Project**

I. Introduction

IN collaboration with CERN, the U.S. High-Luminosity LHC (HL-LHC) Accelerator Upgrade Project is developing low-β quadrupole magnets (MQXFA) to be installed at the interaction region of the LHC [1]–[4] based on a decade-long U.S. LHC Accelerator Research Program (LARP) [5]–[7]. Each Nb_3Sn MQXFA magnet has a magnetic length of 4.2 m with an aperture of 150 mm, generating a nominal operating gradient of 132.6 T/m at 1.9 K, with a peak field of 11.4 T on conductor [2]. The project will deliver 20 MQXFA magnets in 10 cold masses over the next 6 years.

The MQXFA magnets need to meet stringent requirements on field quality at the nominal operating condition [2]. Compared to the NbTi accelerator magnet technology, the Nb_3Sn magnet technology needs to address additional challenges to demonstrate excellent field qualities. For instance, the thermal expansion of Nb_3Sn Rutherford cables [8], [9] and magnets [8]–[11] during heat treatment require additional space in the reaction tooling to avoid excessive thermal strain that can damage the conductors [8]. The resulting positioning of Nb_3Sn conductors and the coil geometry can be less controlled compared to NbTi cases, leading to undesirable geometric field errors [12]–[21].

Magnetic shims close to the magnet aperture can correct geometric field errors [22], [23]. This strategy was proposed for MQXF magnets by applying shims in the bladder slots [24] and was successfully demonstrated in recent LARP Nb_3Sn HQ magnets [16], [18] and short models of MQXF magnets (MQXFS) [21]. Reasonable correlation between the field errors measured at room temperature and nominal operation level was observed in both HQ and MQXFS magnets [15], [19], [21]. Hence, one can install magnetic shims during the magnet assembly stage based on the field errors measured at room temperature, efficient for magnet production.

Room-temperature field quality measurements can provide additional useful information. First, one can evaluate the positions of the local magnetic center and main field angle along the magnet aperture [25]. The data can be compared to those from the cold mass to understand the evolution of magnetic axis and field angles. Similar measurements were performed on the NbTi low-β quadrupole magnets MQXB for the LHC [26]–[29]. Second, field quality measurement at room temperature is an effective quality assurance tool that can detect small anomaly during the assembly process [21], [30]–[32].

In this paper, we report the field quality measurements of a prototype low-β Nb_3Sn quadrupole magnet, MQXFAP2, during the assembly stage, as a first step toward the routine measurements planned for the MQXFA magnet production. The low-order field errors had amplitudes similar to those observed from earlier HQ and MQXFS magnets. The magnetic center and twist angle in the magnet straight section met the acceptance criteria. Further improvements on the measurement system and protocol will be discussed.

The MQXFA magnets will be one of the first applications of Nb_3Sn accelerator magnets in an accelerator complex [1], [4]. We expect the field-quality measurements of MQXFA

Manuscript received on October 30, 2018. This work was supported by the U.S. Department of Energy, Office of Science, Office of High Energy Physics, through the US LHC Accelerator Research Program (LARP) and the US LHC Accelerator Upgrade Project (AUP), and by the High Luminosity LHC project at CERN.

X. Wang, D. W. Cheng, W. Ghiorso, C. Hernikl, T. Lipton, S. Myers, H. Pan, S. O. Prestemon and G.L. Sabbi are with Lawrence Berkeley National Laboratory, Berkeley, CA 94720. (e-mail: {xrwang, glsabbi}@lbl.gov).

G. Ambrosio, G. Chlachidze, J. DiMarco are with Fermi National Accelerator Laboratory, Batavia, IL 80510. (e-mail: dimarco@fnal.gov)

magnets during the assembly stage to provide useful insight and feedback for large-scale application of Nb_3Sn magnet technology in future circular colliders [33].

II. MQXFAP2 Magnet and Measurement Coordinate System

The MQXFAP2 is the second prototype MQXFA magnet consisting of four coils. It has nominally the same mechanical structure as the first prototype magnet featuring eight separate aluminum shells [3]. No mid-plane shim or asymmetric radial shim was used thanks to the relatively uniform coil size [34].

The magnet was assembled at LBNL with several steps. The magnetic measurements were performed after the pre-load and before the splice box was installed.

Fig. 1 gives the coordinate system for MQXFAP2 as a normal quadrupole. Counterclock-wise rotation gives a positive angle.

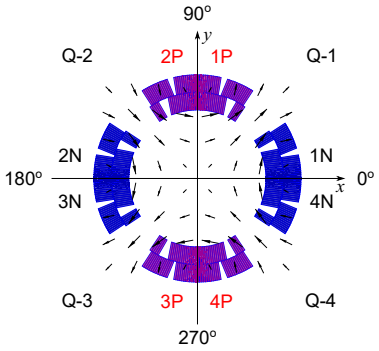

Fig. 1. The coordinate system viewed from the magnet lead end. Each quadrant ("Q") contains one coil. MQXFAP2 had coils 102, 104, 105, 106 from quadrant 1 to 4. Positive current follows the positive z axis toward the reader ("P" for positive and "N" for negative).

Fig. 2 shows the right-handed reference frame for the survey, including the starting frame consistent with Fig. 1, fiducial points, and the laser tracker. The fiducial points were located along the shell edges.

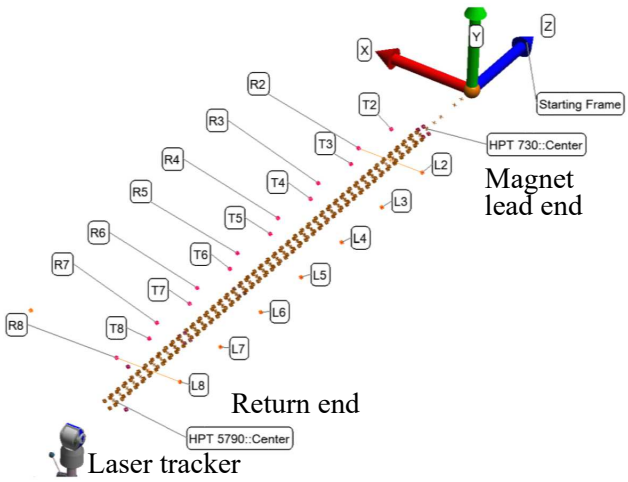

Fig. 2. The reference frame for the survey. Seven groups of fiducial points are shown: L_n, T_n and R_n with $n = 2, \ldots, 8$. The brown points show the locations of four retroreflectors during the scan.

III. Measurement System

We intend to measure three quantities along the magnet aperture with the system: 1) geometric field errors, 2) magnetic center with respect to magnet fiducials, and 3) relative change in the field orientation (twist angle of the main quadrupole field). Similar systems were used for LHC magnets [27], [35], [36].

The measurement system consists of a probe driven rotational and translationally as it slides in a support tube inserted into the magnet aperture. Fig. 3 gives an overview of the measurement system next to the MQXFAP2 magnet.

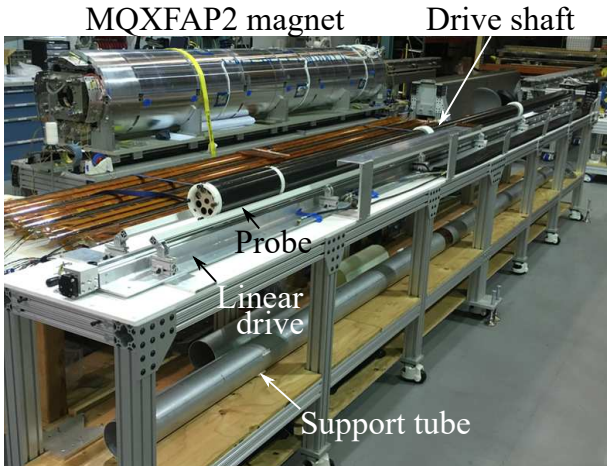

Fig. 3. The measurement system: rotating probe, drive shaft, linear drive, support tube and the rotation drive (not visible). The aluminum shell of the magnet has fiducial features. The data acquisition hardware is not shown.

A. Measurement probe

The measurement probe consists of a rotating coil, support case, slip ring, encoder and rotation motor (Fig. 4). FNAL developed the rotating coil based on the printed-circuit-board (PCB) technology [37]. The coil has two nominally identical PCBs assembled back to back. Each PCB has two layers of traces, delivering the unbucked, dipole-bucked, dipole-quadrupole-bucked voltage signals. A similar rotating coil was used to measure MQXFS1 magnet [19].

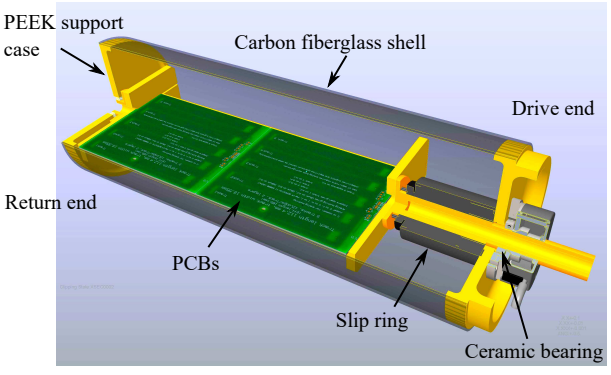

Fig. 4. The CAD rendering of the rotating probe assembly.

A non-magnetic slip ring with 16 channels is used (Moflon, MT2044-S16-N1012). The encoder (Encoder Products Co.,

25T-42SE-1024NV1RHV-SMH) was originally mounted at the probe end but later was moved to the end of the rotation shaft and next to the rotation drive (see § III-B).

A PEEK plastic structure (yellow parts in Fig. 4) supported the PCBs and transferred the rotation torque. A ceramic bearing (Bearing Engineering) was glued at each end of the structure to support the probe rotation with minimal displacement. The whole structure was encapsulated by a carbon fiber tube (Rock West Composites) with an OD of 124.08 mm.

B. Linear and rotation drive

A linear actuator (PBC Linear, MTB055-6300-16B12) drives the probe along the magnet aperture. The linear displacement is controlled by a contactless incremental linear magnetic encoder (RLS LM10ICPRGAA50A00) with a positioning accuracy of about 12 μm.

A segmented carbon fiber push-pull drive shaft (Fig. 3) connected the drive station and the probe. The signal and encoder cables pass through the push-pull tube. A carbon fiber rotation shaft inside the push-pull tube connects the probe to a servo motor (QuickSilver QCI-X23C-6) mounted on the drive station.

Two aluminum pipes of about 3 m length were joined together with Kapton tape to form a full-length support tube (Fig. 3). The tube was inserted into the magnet aperture and was centered at each end of the magnet to support the probe during the measurements. The support tube had an ID of 127 mm and OD of 133.35 mm to maximize the measurement space and protect the instrumentation wires in the aperture.

There are three guide wheels at each end of the probe (Fig. 5). The top wheel is spring-loaded to help center the probe inside the tube.

C. Laser tracker

A laser tracking system (FARO Vantage) was used to measure the position and orientation of the probe with respect to magnet fiducials. This was done with four non-magnetic retroreflectors mounted at the return end of the probe (Fig. 5). The laser tracker was positioned at the return end of the magnet directed toward the probe inside the magnet aperture (Fig. 2).

D. Data acquisition system

The data acquisition system consists of a National Instrument PXI chassis with a 24-bit digitizer (4472B). The sampling rate was 102.4 kHz. During each probe rotation, the voltage signals from the probe and the index and quadrature signals from the encoder are simultaneously digitized and stored in a hard drive for post processing. The probe signals were amplified by a nominal gain of 128. The system is controlled with a LabWindows/CVI program.

The magnet current was measured with a resistive shunt (20 A, 50 mV). The shunt voltage measured by a digital multimeter was recorded manually during the tests.

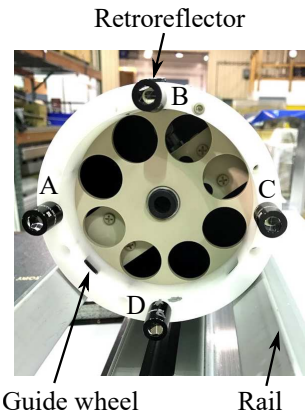

Fig. 5. Four retroreflectors mounted on the return end of the probe housing to determine position and orientation of the probe.

IV. Measurement Protocol and Data Reduction

The measurement coordinate system (Fig. 2) was first established with the laser tracker. Before inserting the probe into the magnet, we measured the stability of the probe rotation axis by tracking a retroreflector that was temporarily glued onto the actual rotating portion of the probe for several rotations. The laser tracker data were fit to a circle. We defined the center of the fit circle as the probe rotation axis. The fitting established the geometric relationship between the coordinates of the four retroreflectors on the probe and the probe rotation axis. The geometric relationship was used to determine the probe axis and orientation during the following scan measurements.

The probe moved from the lead to return end of the magnet in steps of 110 mm. At each location, the probe rotated for 30 rotations at $+15$ A and repeated for -15 A. For both currents, the probe rotated counter-clockwise (viewed from the magnet lead end) at a speed of 3 Hz. The resulting flux data were averaged to minimize the effect of iron and Earth field.

At each scan location, the magnetic center of the magnet with respect to the magnet fiducials was determined based on two sets of data. The first set was the location of the magnetic center with respect to the rotation axis of the probe. This was determined based on the standard procedure of center localization [38]. The second set was the coordinates of the probe axis with respect to the magnet fiducials based on the laser tracker measurements. Summing both data at each location, we obtained the magnetic center of the magnet with respect to the magnet fiducials.

The twist angle at each scan location was also determined based on two sets of data. The first was the main field angle with respect to the encoder index pulse. The second was the change of index angle along the magnet aperture. This was measured in two ways for MQXFAP2: one with a digital protractor (Mitutoyo Pro3600) mounted on the encoder; the other was measured by the laser tracker system assuming negligible torsion over the entire length of the carbon fiber pusher tube. We obtained the relative change of the twist angle by summing both data sets.

The magnetic field in the aperture of the quadrupole magnet

is expressed as a series expansion given by

$$B_y + iB_x = B_2 \times 10^{-4} \sum_{n=1}^{\infty} (b_n + ia_n) \left(\frac{x+iy}{R_{\text{ref}}} \right)^{n-1}, \quad (1)$$

where b_n is the normal and a_n is the skew multipole coefficient of order n. They are normalized to the main field (B_2) at the magnet center and are expressed in units at the reference radius $R_{\text{ref}} = 50$ mm [39].

V. Test Results

A. Probe performance

A total of 580 data points were collected by tracking the temporary retroreflector on the rotating probe. The least-square fit to a circle gave a maximum radial deviation of 25 μm with an RMS standard deviation of 15 μm.

Following the analysis in [19], we found the probe had a resolution of about 0.003 units at the reference radius, consistent with an earlier probe used for the warm measurements of MQXFS magnets [19].

B. Main field and low-order field errors

Fig. 6 plots the main field transfer function along the magnet. The mechanical center of the magnet shell (fiducial #5 in Fig. 2) was set to $z = 0$. The magnetic straight section was within -2 and 1.7 m.

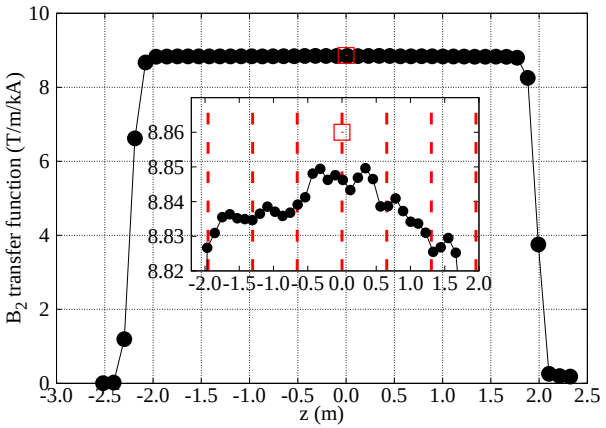

Fig. 6. The main field transfer function along the magnet aperture. Measurements: black circles. 2D calculation: red square. The vertical red lines in the inset indicate the locations of shell edges.

Fig. 7 shows the b_3, b_4 and b_5 along the magnet aperture normalized to the main field at the magnet center. Fig. 8 shows the skew counterparts.

Table I gives the mean value and the standard deviation of the low-order field errors in the magnetic straight section.

TABLE I
THE MEAN VALUE (μ) AND STAND DEVIATION (σ) OF FIELD ERRORS IN THE MAGNETIC STRAIGHT SECTION. $R_{\text{REF}} = 50$ MM.

	b_3	b_4	b_5	b_6	a_3	a_4	a_5	a_6
μ	-1.68	-1.15	-0.46	-5.50	3.42	1.99	1.93	0.69
σ	2.08	1.33	1.11	2.19	2.00	2.35	0.92	0.77

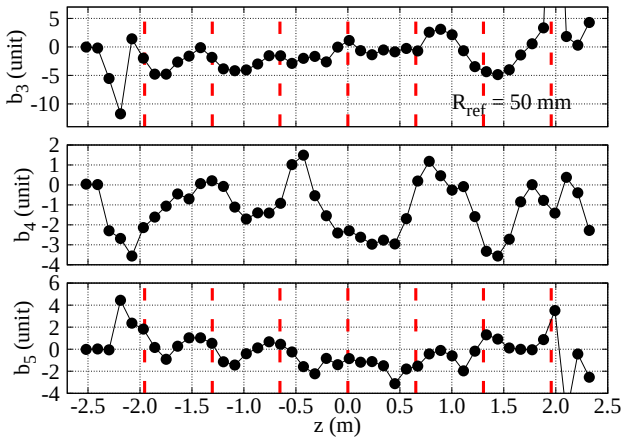

Fig. 7. The normal sextupole, octupole and decapole harmonics along the magnet aperture within the magnet straight section. The vertical red lines indicate the locations of shell edges.

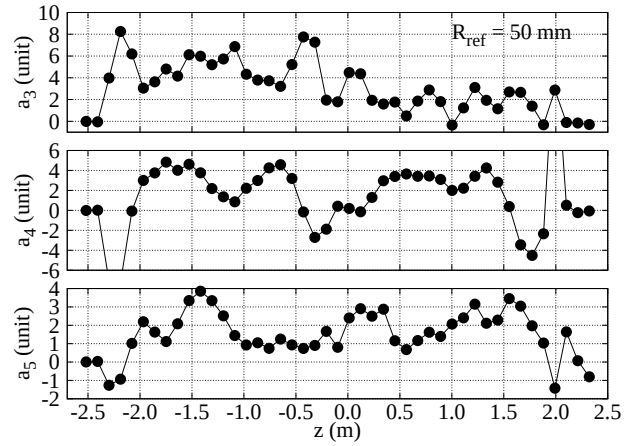

Fig. 8. The skew sextupole, octupole and decapole harmonics along the magnet aperture.

C. Magnetic centers

We considered two reference axes to determine and analyze the magnetic centers along MQXFAP2. The first was a straight axis defined by two points: M_8, the mid-point between fiducial L_8 and R_8 and M_2, the mid-point between fiducial L_2 and R_2 (Fig. 2). The second axis was a piecewise straight line by connecting the midpoints M_{n+1} and M_n with n ranging from 2 to 7.

Fig. 9 shows the (x, y) coordinates of the magnetic center along the magnet aperture with respect to two reference axes. In both cases, the magnetic center was within ± 0.5 mm from the reference axis both in horizontal and in vertical directions. That the two references axes do not coincide is discussed further in § VI.

D. Relative change of the main field twist angle

Fig. 10 shows the relative change of the twist angle along the magnet aperture. One set of data was based on the angle measured at the encoder end by the digital protractor and the other set was based on the laser tracker measurements at the probe end.

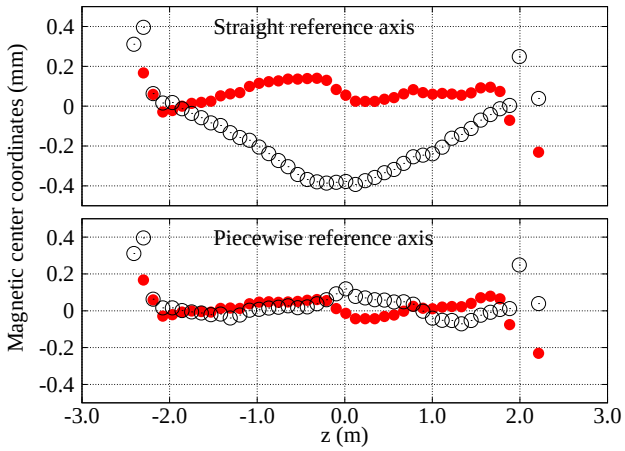

Fig. 9. The coordinates of the magnetic center along the magnet aperture. x: red solid circles. y: black open circles.

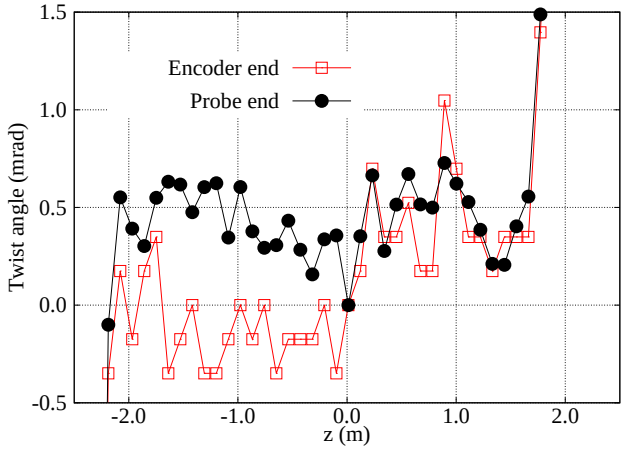

Fig. 10. The twist angle along the magnet aperture. The angle was shifted to have zero value at $z = 0$.

Table II gives the mean, maximum and minimum twist angle in the magnetic straight section. The twist angle was within the required ± 2 mrad of the mean value [25].

TABLE II
THE MEAN VALUE (μ), MAXIMUM AND MINIMUM TWIST ANGLE IN THE MAGNETIC STRAIGHT SECTION. UNIT: MRAD.

	Encoder side	Probe side
μ	0.14	0.47
max	1.40	1.49
min	-0.35	0.00

VI. Discussion

The main field transfer function increased by 0.1% in the center part of the magnet between ± 0.5 m compared to the rest of the straight section. An independent measurement at room temperature at Brookhaven National Laboratory showed similar results [40]. The cause for this profile remains to be clarified.

The low-order geometric errors were not negligible. The amplitude and variation of the field errors were similar to HQ and MQXFS magnets [16], [18], [19], [21]. The amplitude averaged along the magnet straight section was within the correction capability of magnetic shims placed in bladder slots [16], [21].

There seems to be a correlation between the variation of field harmonics (the transfer function, b_3 and b_5) and the segmented Aluminum shells (Figs. 6 and 7). To confirm this correlation, one can measure, for instance, the coil pack before insertion into the magnet structure.

Although the deviation of the magnetic centers in the y direction peaked at the magnet center for about 0.4 mm (Fig. 9), it was still within the 0.5 mm limit specified in the acceptance criterion. The magnet geometry contributed partially to the V-shaped y-coordinate curve with respect to the straight reference axis. This was demonstrated by using the piecewise reference axis which considered the fiducials on the magnet. Dedicated survey measurements on the assembly table showed that the table deformed with the magnet [34]. This contributed to the magnet deformation and will be corrected [34].

The laser tracker and protractor gave consistent measurement of the angle of the encoder index pulse. The large uncertainty of the protractor (± 0.873 mrad) may contribute to the difference between the two methods.

The output voltage of the power supply increased during the measurements, indicating the warmup of the magnet (the power generation was 563 W). The potential temperature gradient in the magnet aperture can deflect light and affect the measurement of magnetic center [41].

Based on the feedback from the first measurements reported here, the following items will be implemented or studied for the future measurements during the assembly stage of MQXF magnets:

1) Record the magnet current with a direct current current transformer. Measure the angle more accurately at the encoder end.
2) Move the probe in steps of the actual effective length of the PCB circuit to facilitate the integral measurements.
3) Measure the field quality at different assembly stages: the coil pack before insertion into the iron yoke, before loading, and after loading with the lead-end splice box completed.
4) Measure the temperature gradient in the magnet aperture and understand its impact on the light deflection.

VII. Conclusion

The U.S. High-Luminosity Upgrade Project plans to measure the field quality of Nb_3Sn low-β quadrupole magnets (MQXFA) during the magnet assembly stage. The measurements can facilitate the correction of geometric field errors, if necessary. In addition, the magnetic center and main field twist angles will be measured to determine if the magnets meet the acceptance criteria. We measured a prototype 4.2-m long magnet (MQXFAP2) with a prototype measurement system. The magnet showed non-negligible low-order geometric field errors that were correctable with magnetic shims. In the magnet straight section, the magnetic centers were within ± 0.5 mm of the external fiducial axis and the main field twist angle

was within ± 2 mrad of the averaged twist angle. Further improvements on measurement hardware and protocol were identified. We expect the planned field quality measurements to provide useful insight for large-scale application of Nb_3Sn accelerator magnets for future circular colliders.

ACKNOWLEDGMENT

We thank Adam Balogh, Joshua Herrera and Ahmet Pekedis of LBNL for their support on part fabrication and magnet test.

REFERENCES

[1] G. Ambrosio, "Nb_3Sn high field magnets for the high luminosity LHC upgrade project," *IEEE Trans. Appl. Supercond.*, vol. 25, no. 3, p. 4002107, June 2015.

[2] P. Ferracin, G. Ambrosio, M. Anerella *et al.*, "Development of MQXF: The Nb_3Sn low-β quadrupole for the HiLumi LHC," *IEEE Trans. Appl. Supercond.*, vol. 26, no. 4, p. 4000207, 2016.

[3] D. W. Cheng, G. Ambrosio, E. C. Anderssen *et al.*, "Fabrication and assembly performance of the first 4.2 m MQXFA magnet and mechanical model for the Hi-Lumi LHC upgrade," *IEEE Trans. Appl. Supercond.*, vol. 28, no. 3, p. 4006207, Apr. 2018.

[4] E. Todesco, M. Annarella, G. Ambrosio *et al.*, "Progress on HL-LHC Nb_3Sn magnets," *IEEE Trans. Appl. Supercond.*, vol. 28, no. 4, p. 4008809, Jun. 2018.

[5] S. Gourlay, G. Ambrosio, N. Andreev *et al.*, "Magnet R&D for the US LHC accelerator research program (LARP)," *IEEE Trans. Appl. Supercond.*, vol. 16, no. 2, pp. 324–327, 2006.

[6] P. Ferracin, "LARP Nb_3Sn quadrupole magnets for the LHC luminosity upgrade," *Advances in Cryogenic Engineering—Transactions of the Cryogenic Engineering Conference*, vol. 55, pp. 1291–1300, 2010.

[7] G. Sabbi, "Nb_3Sn IR quadrupoles for the high luminosity LHC," *IEEE Trans. Appl. Supercond.*, vol. 23, no. 3, p. 4000707, 2013.

[8] H. Felice, G. Ambrosio, M. Anerella *et al.*, "Impact of coil compaction on LARP HQ magnet," *IEEE Trans. Appl. Supercond.*, vol. 22, no. 3, p. 4001904, 2012.

[9] E. Rochepault, P. Ferracin, G. Ambrosio *et al.*, "Dimensional changes of Nb_3Sn Rutherford cables during heat treatment," *IEEE Trans. Appl. Supercond.*, vol. 26, no. 4, p. 4802605, Jun. 2016.

[10] D. R. Chichili, G. Ambrosio, N. Andreev *et al.*, "Fabrication of the shell-type Nb_3Sn dipole magnet at Fermilab," *IEEE Trans. Appl. Supercond.*, vol. 11, no. 1, pp. 2160–2163, Mar. 2001.

[11] G. Ambrosio, N. Andreev, M. Anerella *et al.*, "Development and coil fabrication for the LARP 3.7-m long Nb_3Sn quadrupole," *IEEE Trans. Appl. Supercond.*, vol. 19, no. 3, pp. 1231–1234, Jun. 2009.

[12] G. V. Velev, G. Ambrosio, N. Andreev *et al.*, "Field quality study of the LARP Nb_3Sn 3.7 m-long quadrupole models of LQ series," *IEEE Trans. Appl. Supercond.*, vol. 22, no. 3, p. 9002804, Jun. 2012.

[13] G. Chlachidze, J. DiMarco, N. Andreev *et al.*, "Field quality study of a 1-m-long single-aperture 11-T Nb_3Sn dipole model for LHC upgrades," *IEEE Trans. Appl. Supercond.*, vol. 24, no. 3, p. 4000905, Jun. 2014.

[14] L. Fiscarelli, M. Giovannozzi, P. D. Hermes *et al.*, "Field quality of MBH 11-T dipoles for HL-LHC and impact on beam dynamic aperture," *IEEE Trans. Appl. Supercond.*, vol. 28, no. 3, p. 4004005, Apr. 2018.

[15] J. DiMarco, G. Ambrosio, M. Buehler *et al.*, "Field quality measurements of LARP Nb_3Sn magnet HQ02," *IEEE Trans. Appl. Supercond.*, vol. 24, no. 3, p. 4003905, 2014.

[16] J. DiMarco, G. Ambrosio, M. Anerella *et al.*, "Test results of the LARP Nb_3Sn quadrupole HQ03a," *IEEE Trans. Appl. Supercond.*, vol. 26, no. 4, p. 4005105, Jun. 2016.

[17] E. F. Holik, G. Ambrosio, A. Carbonara *et al.*, "Field quality and fabrication analysis of HQ02 reconstructed Nb_3Sn coil cross sections," *IEEE Trans. Appl. Supercond.*, vol. 27, no. 4, p. 4003405, Jun. 2017.

[18] X. Wang, G. Ambrosio, G. Chlachidze *et al.*, "Analysis of field errors for LARP Nb_3Sn HQ03 quadrupole magnet," *IEEE Trans. Appl. Supercond.*, vol. 27, no. 4, p. 4000805, Jun. 2017.

[19] J. DiMarco, G. Ambrosio, G. Chlachidze *et al.*, "Magnetic measurements of the first Nb_3Sn model quadrupole (MQXFS) for the High-Luminosity LHC," *IEEE Trans. Appl. Supercond.*, vol. 27, no. 4, p. 9000105, Jun. 2017.

[20] L. Fiscarelli, H. Bajas, O. Dunkel *et al.*, "Magnetic measurements on the first CERN-built models of the insertion quadrupole MQXF for HL-LHC," *IEEE Trans. Appl. Supercond.*, vol. 28, no. 3, p. 4002605, Apr. 2018.

[21] S. Izquierdo Bermudez, G. Ambrosio, H. Bajas *et al.*, "Geometric field errors of short models for MQXF, the Nb_3Sn low-β quadrupole for the high luminosity LHC," *IEEE Trans. Appl. Supercond.*, vol. 28, no. 3, p. 4006306, Apr. 2018.

[22] R. Gupta, M. Anerella, J. Cozzolino *et al.*, "Tuning shims for high field quality in superconducting magnets," *IEEE Transactions on Magnetics*, vol. 32, no. 4, pp. 2069–2073, 1996.

[23] G. Sabbi, J. DiMarco, A. Nobrega *et al.*, "Correction of high gradient quadrupole harmonics with magnetic shims," *IEEE Trans. Appl. Supercond.*, vol. 10, no. 1, pp. 123–126, 2000.

[24] P. Hagen, "Study of fine-tuning field quality in MQXF quadrupole," CERN, Tech. Rep., November 2014, HiLumi LHC Milestone Report 36.

[25] R. Carcagno, G. Sabbi, and P. Ferracin, "US HL-LHC accelerator upgrade project acceptance criteria part A: MQXFA magnet," 2018, US-HiLumi-doc-1103.

[26] H. Hirano, N. Ohuchi, Y. Ajima *et al.*, "Warm magnetic field measurements of prototype low-β quadrupole magnet MQXA for the LHC interaction regions," *IEEE Trans. Appl. Supercond.*, vol. 12, no. 1, pp. 1663–1666, Mar. 2002.

[27] H. Hirano, N. Ohuchi, Y. Ajima *et al.*, "Measurements of magnetic axis and twist of a low-beta quadrupole magnet for LHC by using a morgan coil," in *Particle accelerator. Proceedings, 8th European Conference, EPAC 2002, Paris, France, June 3-7, 2002*, 2002, pp. 2400–2402.

[28] N. Ohuchi, Y. Ajima, T. Nakamoto *et al.*, "Magnetic field measurements of the LHC-IR MQXA magnets at room temperature," *IEEE Trans. Appl. Supercond.*, vol. 14, no. 2, pp. 239–242, Jun. 2004.

[29] G. V. Velev, R. Bossert, R. Carcagno *et al.*, "Magnetic field measurements of LHC inner triplet quadrupoles fabricated at Fermilab," *IEEE Trans. Appl. Supercond.*, vol. 17, no. 2, pp. 1109–1112, Jun. 2007.

[30] R. Gupta, M. Anerella, J. Cozzolino *et al.*, "Field quality analysis as a tool to monitor magnet production," in *Proceedings of 15th International Conference on Magnet Technology*, 1997.

[31] A. Jain, "Measurements as a tool to monitor magnet production," https://www.bnl.gov/magnets/Staff/Gupta/scmag-course/uspas03/AJ03/AJ_ProductionTool.pdf, 2003.

[32] B. Bellesia, G. Molinari, C. Santoni *et al.*, "Short circuit localization in the LHC main dipole coils by means of room temperature magnetic measurements," *IEEE Trans. Appl. Supercond.*, vol. 16, no. 2, pp. 208–211, Jun. 2006.

[33] L. Bottura, G. de Rijk, L. Rossi *et al.*, "Advanced accelerator magnets for upgrading the LHC," *IEEE Trans. Appl. Supercond.*, vol. 22, no. 3, p. 4002008, 2012.

[34] D. Cheng, G. Ambrosio, E. Anderssen *et al.*, "Mechanical performance of the first prototype 4.5 m long Nb_3Sn low-β quadrupole magnets for the Hi-Lumi LHC upgrade," This conference, 2018.

[35] J. G. Perez, J. Billan, M. Buzio *et al.*, "Performance of the room temperature systems for magnetic field measurements of the LHC superconducting magnets," *IEEE Trans. Appl. Supercond.*, vol. 16, no. 2, pp. 269–272, Jun. 2006.

[36] G. V. Velev, R. Bossert, R. Carcagno *et al.*, "Field quality of the LHC inner triplet quadrupoles being fabricated at fermilab," in *Proceedings of the 2003 Particle Accelerator Conference*, vol. 3, May 2003, pp. 1969–1971.

[37] J. DiMarco, G. Chlachidze, A. Makulski *et al.*, "Application of PCB and FDM technologies to magnetic measurement probe system development," *IEEE Trans. Appl. Supercond.*, vol. 23, no. 3, p. 9000505, 2013.

[38] L. Bottura, "Standard analysis procedures for field quality measurement of the LHC magnets — part I: harmonics," LHC/MTA, Tech. Rep. LHC-MTA-IN-97-007, 2001.

[39] A. K. Jain, "Basic theory of magnets," in *CERN Accelerator School: measurement and alignment of accelerator and detector magnets*, 1998, no. CERN-98-05, pp. 1–26.

[40] H. Song, J. DiMarco, A. Jain *et al.*, "Vertical magnetic measurement system commissioning and first measurements of the first full-length prototype quadrupole magnet for the LHC Hi-Lumi upgrade," this conference, 2018.

[41] P. Schnizer, G. Deferne, M. Dupont *et al.*, "Experience from measuring the LHC quadrupole axes," in *Proceedings of the 8th International Workshop on Accelerator Alignment (IWAA)*, 2004.